Supporting Information

Transient Absorption Spectrum Analysis for Photothermal Catalysis Perovskite Materials

Jindan Tian[1*], Lili Liu[1], Hongqiang Nian[1], Qiangsheng Guo[2], Na Sha[2,*] and Zhe Zhao [1,*]

[1]School of Material Science and Engineering, Shanghai Institute of Technology, Shanghai 201418, China

[2]School of Chemical and Environment Engineering, Shanghai Institute of Technology, Shanghai 201418, China

*To whom correspondence should be addressed.

E-mail: tjd@sit.edu.cn (J.T.); shana@sit.edu.cn (N.S.); zhezhao@sit.edu.cn (Z.Z.)

Contents of the Supporting Information

Figure S7. The XPS spectra of (a) Co 2p, (b) Mn 2p, (c) Ni 2p, (d) O 1s of LCMO and LNCO

Figure S8. Two exponential decay function and fitting curve of $LaCo_{0.6}Mn_{0.4}O_3$

Figure S9. The error of lifetime of LCMO, LMNO and LNCO

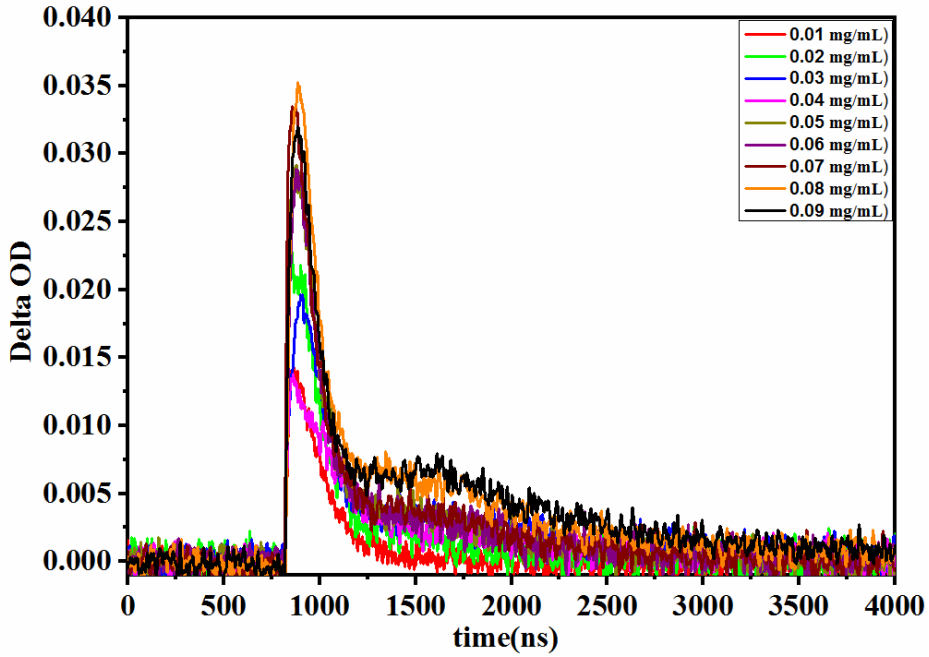

Figure S1. The different concentrations of the decay curve in $LaMn_{0.6}Ni_{0.4}O_3$

Figure S1 exhibited the different concentrations of the decay curve in $LaMn_{0.6}Ni_{0.4}O_3$. It can be found when the concentration is too high or too low, significantly influencing the dynamic decay curve. Because catalysts are black powder, so when the concentration is too high, on the one hand, the solution is too dark for light transmission and prone to sedimentation; on the other hand, it will cause excessive carrier generation during excitation. It is well known that excessive carrier caused faster recombination or secondary excitation; the concentration is too low that excited few carriers are unsuitable for carrier monitoring. Finally, 0.05mg/mL was chosen to be the optimal concentration.

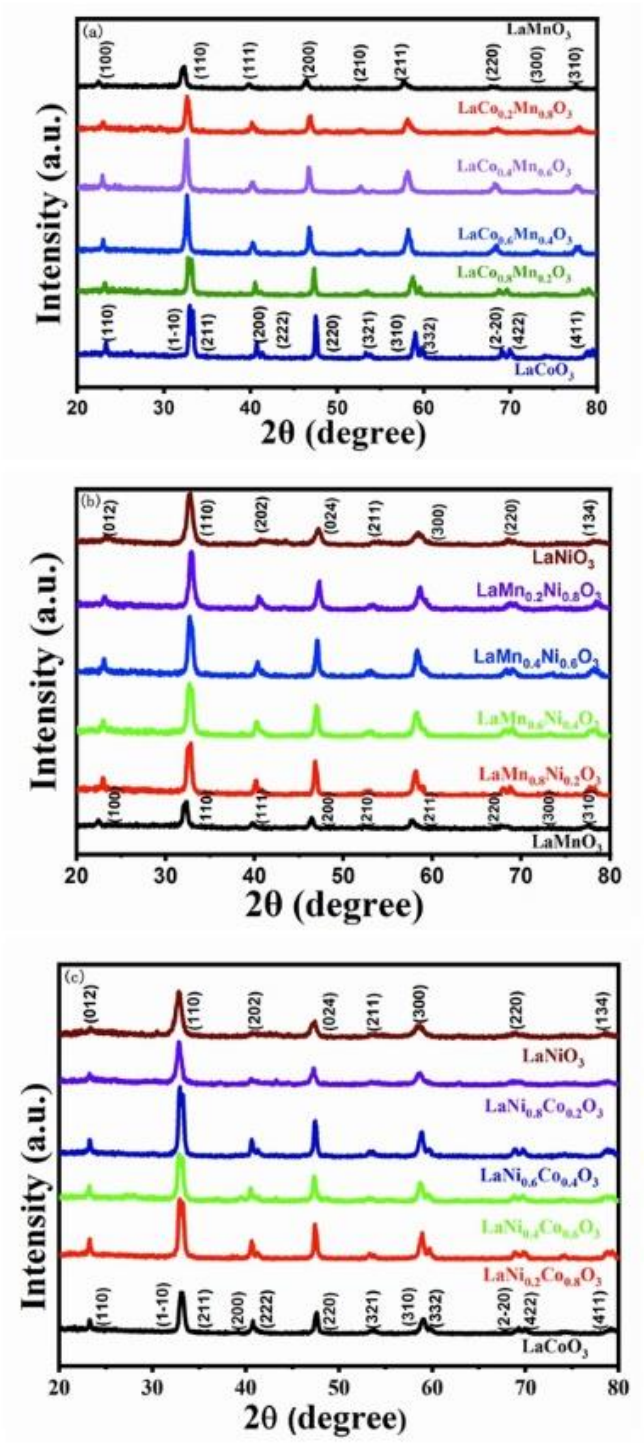

Figure S2. XRD patterns of perovskite a) LCMO, b) LMNO, c) LNCO (x = 0, 0.2, 0.4, 0.6, 0.8, 1.0)

Fig. S2 shows the X-ray diffraction (XRD) of LCMO, LMNO and LNCO. All catalysts were confirmed to be a pure phase with no impurities, stating that Co, Mn and Ni were successfully doped at B-sites to form a solid solution. However, the crystal shape, peak width, peak position and peak strength all change with the doping of different elements and ratios, which indicates that doping can change the crystallinity and lattice parameters. When the peak shift to a high angle means that the doping ion radius is smaller than the original metal ion. The Scherer method calculated the lattice size of LCMO, LMNO and LNCO. It was found that $LaCo_{0.6}Mn_{0.4}O_3$,

$LaMn_{0.6}Ni_{0.4}O_3$ and $LaNi_{0.6}Co_{0.4}O_3$ have the smallest lattice size in three series, which indicated the maximum lattice distortion. The distortion of perovskite crystal structure indicated that the crystal had higher system energy, while the higher system energy had higher catalytic activity. All in all, doping would be caused crystal lattice defects to promote the adsorption of reactants.

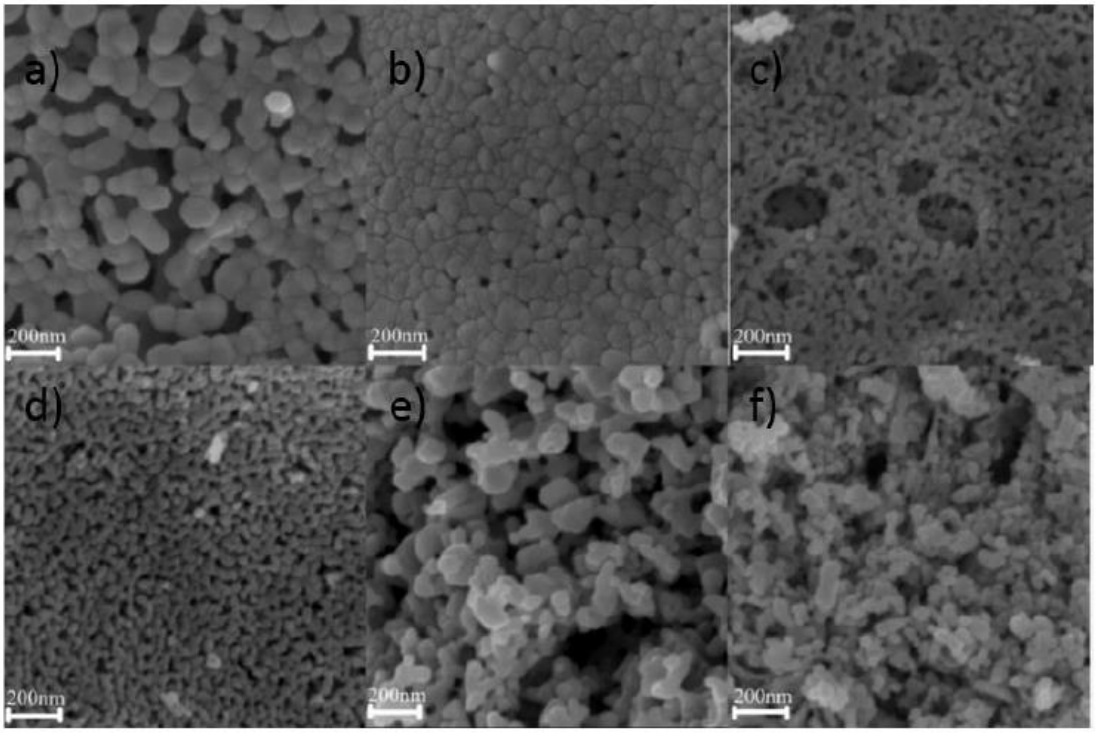

Figure S3. SEM images of LCMO powers synthesized by sol-gel combustion method at 700°C for 7h. a) x = 0, b) x = 0.2, c) x = 0.4, d) x = 0.6, e) x = 0.8, f) x = 1.0.

SEM characterized the morphological features. It can be seen that all samples are porous material. Porous materials are beneficial to CO_2 adsorption and promote surface reactions. For LCMO, when x=0, 0.8, 1, the particle size is relatively uneven, and there are many aggregations. When Co=0.2, 0.4, 0.6, the particle size gradually becomes uniform with less agglomeration, the porosity increases correspondingly, and the pores between particles are connected to each other. It can be clearly seen that x=0.6 shows the best morphology, and the overall distribution of x=0.6 is the pore structure formed by the connection of particles, which is conducive to the storage and transmission of reaction products in the catalytic reaction. LMNO and LNCO have similar laws; we will not list them here.

Table S1. The BET analysis and CH_4 yield of LCMO, LMNO and LNCO (x = 0, 0.2, 0.4, 0.6, 0.8, 1.0)

Sample	Surface area (BET) m^2/g	Pore size (nm)	CH_4 yield(umol/g)
$LaCoO_3$	21.99	17.651	130.65
$LaCo_{0.2}Mn_{0.8}O_3$	9.12	18.39	349.87
$LaCo_{0.4}Mn_{0.6}O_3$	22.82	23.43	471.90
$LaCo_{0.6}Mn_{0.4}O_3$	19.51	27.43	510.68
$LaCo_{0.8}Mn_{0.2}O_3$	10.80	20.38	250.96
$LaMnO_3$	21.99	17.65	340.49
$LaMn_{0.2}Ni_{0.8}O_3$	10.56	18.39	342.31
$LaMn_{0.4}Ni_{0.6}O_3$	15.57	23.43	429.59
$LaMn_{0.6}Ni_{0.4}O_3$	21.60	27.43	573.26
$LaMn_{0.8}Ni_{0.2}O_3$	22.22	20.38	291.55
$LaNiO_3$	4.11	30.38	107.80
$LaNi_{0.2}Co_{0.8}O_3$	10.06	30.42	187.43
$LaNi_{0.4}Co_{0.6}O_3$	13.40	23.27	164.17
$LaNi_{0.6}Co_{0.4}O_3$	6.51	36.90	358.52
$LaNi_{0.8}Co_{0.2}O_3$	2.66	34.75	348.91

Table S1 shows the specific surface area, pore diameter and CH4 yield of LCMO, LMNO and LNCO catalysts. The specific surface area at 4.11~22.82 m^2/g can be considered a porous material. It can be seen from table S1 that the pore size changes with the doping value, but there is no consistent trend among different materials. Compared to pure $LaNiO_3$, $LaCoO_3$ and $LaMnO_3$, the influence of doping on the specific surface area has no particular law. However, for the most part, doping can effectively increase the specific surface area of the catalyst. From the catalytic results, the specific surface area does not correspond to the catalytic activity of the catalyst, so it can be said that the specific surface area cannot be used as a primary factor to judge the catalytic activity.

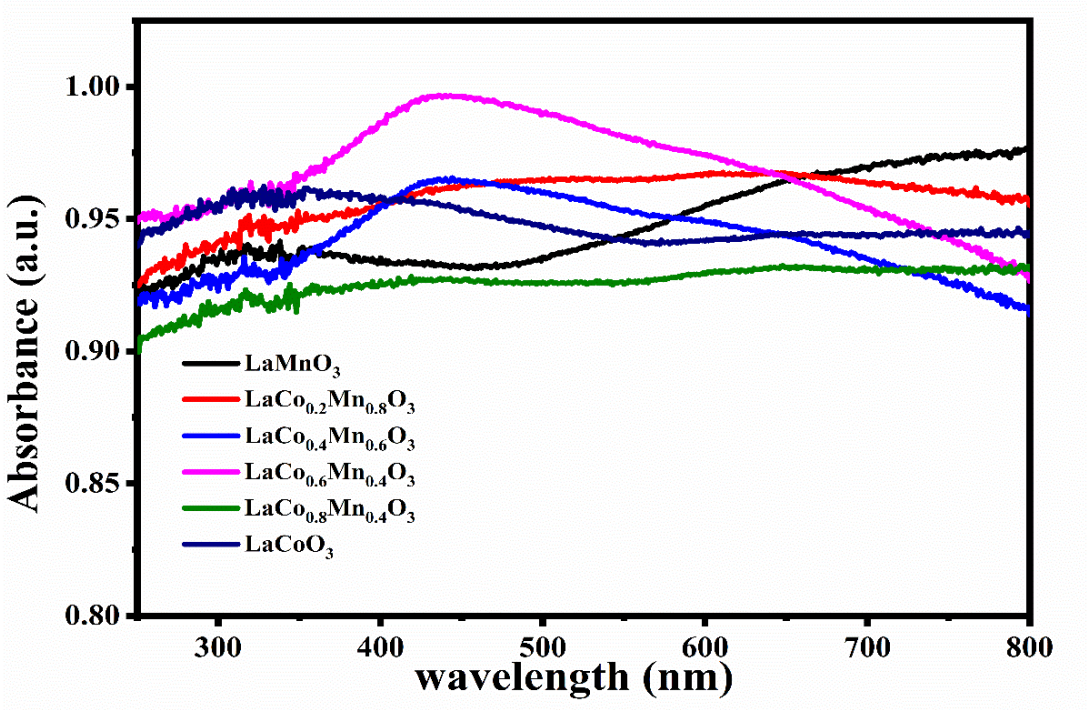

Figure S4. UV-vis diffuse reflectance spectra of the LCMO powders (x = 0, 0.2, 0.4, 0.6, 0.8, 1.0)

In the LCMO UV-diffuse reflectance spectrum, it can be seen that the compounds show strong absorption in the wavelength range of 200-800nm, which means that the catalyst has a strong response from UV to visible light. In other words, the catalysts have a solid response to visible light, representing that visible light can ultimately drive photocatalytic reactions. The same is true of the other two series (LMNO, LNCO)

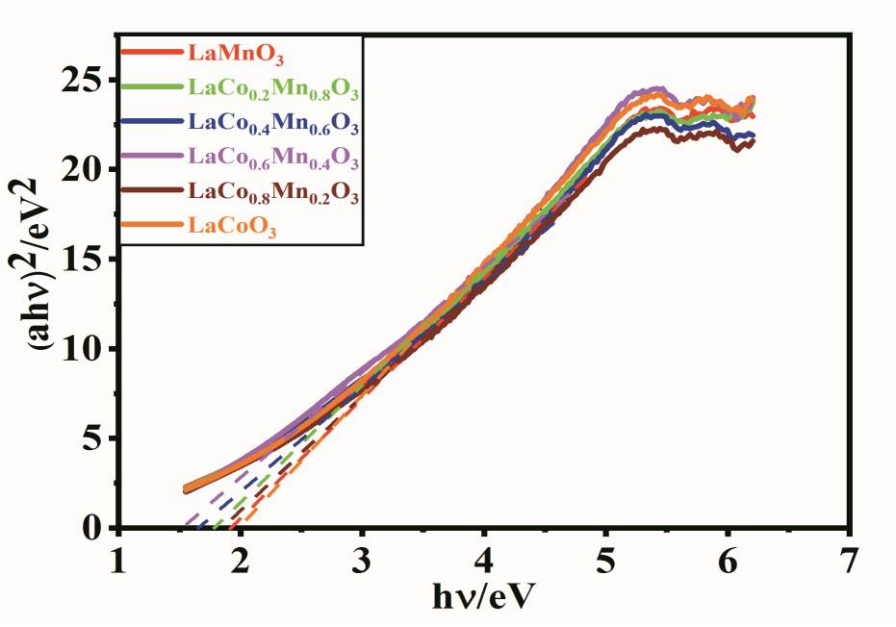

Figure S5. The energy gap of the LCMO powders (x = 0, 0.2, 0.4, 0.6, 0.8, 1.0)

To estimate the catalysts' optical band gap (Eg), the Tauc equation was used to fit E_g of the catalysts**.** Fig. S5 shows the Eg of LCMO powders. As far as we know, Eg not only

determines the choice of the photo-responsive region but also reflects the mobility of electrons from the valence to the conduction band. Lower E_g can absorb visible light more effectively and facilitate the separation of electrons-holes pairs from the valence to the conduction band, potentially improving the photocatalytic performance. Obviously, B-doping can effectively reduce E_g.

Table S2. The Eg, CB, VB and CH_4 yield of LCMO, LMNO and LNCO (x = 0, 0.2, 0.4, 0.6, 0.8, 1.0)

Sample	Eg (eV)	CB	VB	CH_4 yield(umol/g)
$LaCoO_3$	1.86	-0.31	1.55	130.65
$LaCo_{0.2}Mn_{0.8}O_3$	1.68	-0.28	1.40	349.87
$LaCo_{0.4}Mn_{0.6}O_3$	1.77	-0.26	1.51	471.90
$LaCo_{0.6}Mn_{0.4}O_3$	1.38	-0.30	1.08	510.68
$LaCo_{0.8}Mn_{0.2}O_3$	1.81	-0.27	1.54	250.96
$LaMnO_3$	1.83	-0.24	1.59	340.49
$LaMn_{0.2}Ni_{0.8}O_3$	1.79	-0.27	1.52	342.31
$LaMn_{0.4}Ni_{0.6}O_3$	1.82	-0.28	1.54	429.59
$LaMn_{0.6}Ni_{0.4}O_3$	1.50	-0.24	1.26	573.26
$LaMn_{0.8}Ni_{0.2}O_3$	1.52	-0.24	1.28	291.55
$LaNiO_3$	1.78	-0.27	1.51	107.80
$LaNi_{0.2}Co_{0.8}O_3$	1.48	-0.25	1.23	187.43
$LaNi_{0.4}Co_{0.6}O_3$	1.42	-0.24	1.18	164.17
$LaNi_{0.6}Co_{0.4}O_3$	1.45	-0.25	1.20	358.52
$LaNi_{0.8}Co_{0.2}O_3$	1.69	-0.26	1.13	348.91

The CB was fitted by the mott-Schottky diagram (**Figure S6**), and the Eg value was obtained by DRS spectral. The VB value can also be calculated through the formula $E_{CB} = E_{VB} - E_g$. Tab. S2 showed the Eg, CB and VB values of all B-doped solid solution catalysts, which indicated that B-doped catalysts had lower Eg than those of the pure catalysts. From the catalytic results, the value of Eg does not correspond to the catalytic activity. This conclusion is similar to the results of BET. It can be concluded that there is a specific relationship between the Eg and the catalytic activity.

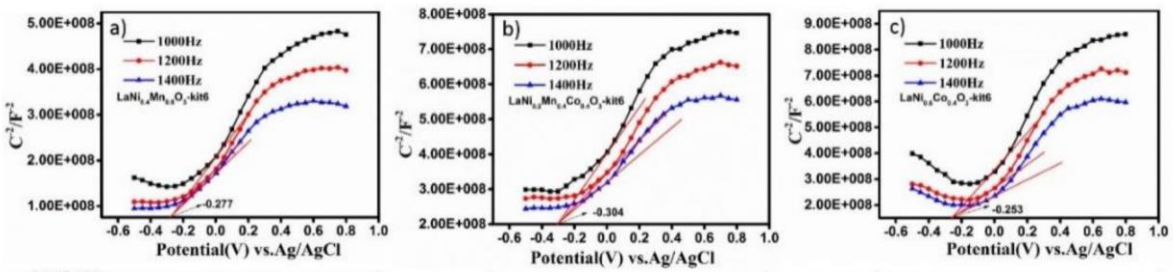

Figure S6. Mott–Schottky plots of $LaNi_{0.4}Mn_{0.6}O_3$, $LaCo_{0.6}Mn_{0.4}O_3$, $LaNi_{0.6}Co_{0.4}O_3$

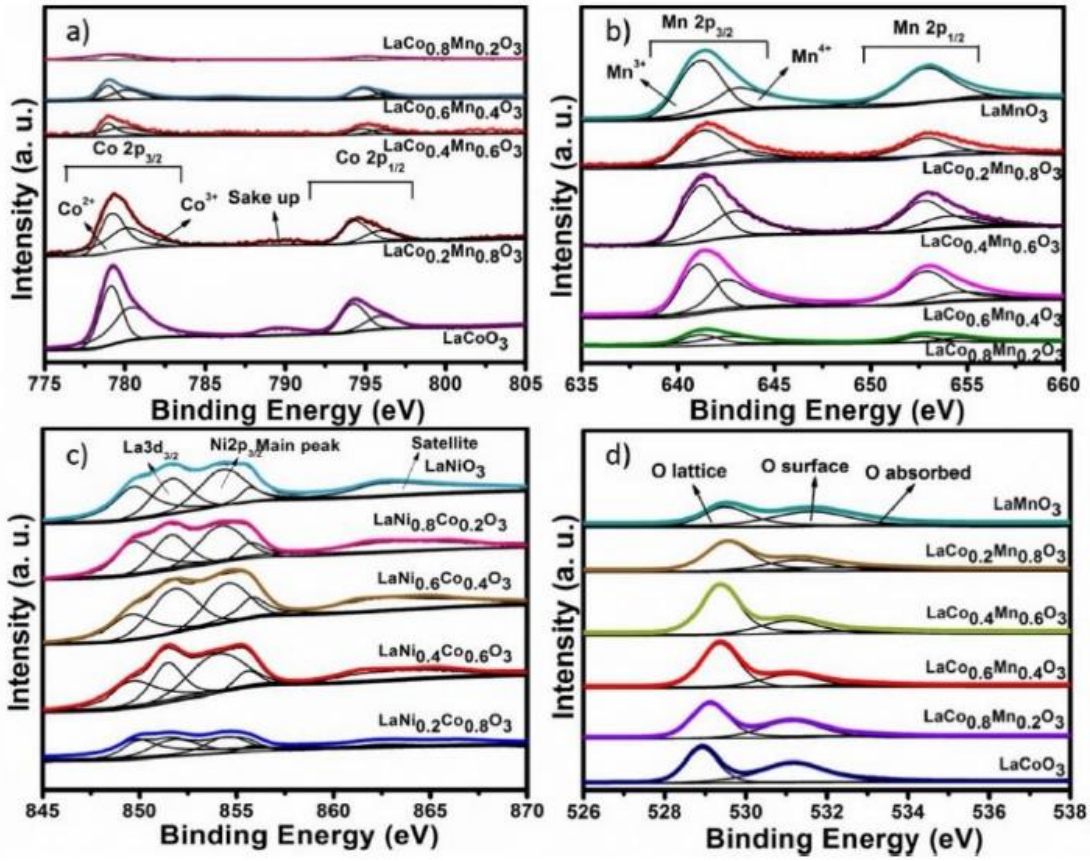

Figure S7. The XPS spectra of (a) Co 2p, (b) Mn 2p, (c) Ni 2p, (d) O 1s of LCMO and LNCO

As shown in Fig. S7, the chemical valence and surface morphology of the elements in LCMO, LMNO and LNCO catalysts were analyzed by XPS. The results show that the elements contained La, Co, Mn, Ni, O and C in all samples, and no peaks of other elements appear. The binding energy in the spectrum proves that there are at least two oxidation states of ions. As shown in the Fig. S7a, Co exists in two oxidation states, Co^{2+} and Co^{3+}. High binding energy corresponds to $Co^{3+,}$ and low binding energy corresponds to Co^{2+}. Similarly, two major peaks corresponding to Mn 2p $_{3/2}$ and Mn 2p $_{1/2}$ were observed at 641.8 and 653.5eV, respectively (Fig. S7b). The strength of peak Mn^{4+} increased with the doping ratio, while the Mn^{3+} showed an opposite trend to balance the charge. Because the binding energy of the Ni 2p $_{3/2}$ peak is almost the same as that of the satellite peak of La 3d $_{3/2}$ in LNCO, these peaks overlap, analyzing Ni ion valences difficult (Fig. S7c). Oxygen has three oxidation states: lattice oxygen, surface oxygen and adsorbed oxygen (Fig. S5d). The surface oxygen increased with the different doping ratios, which indicates that doping can effectively improve the adsorption capacity of reactants.

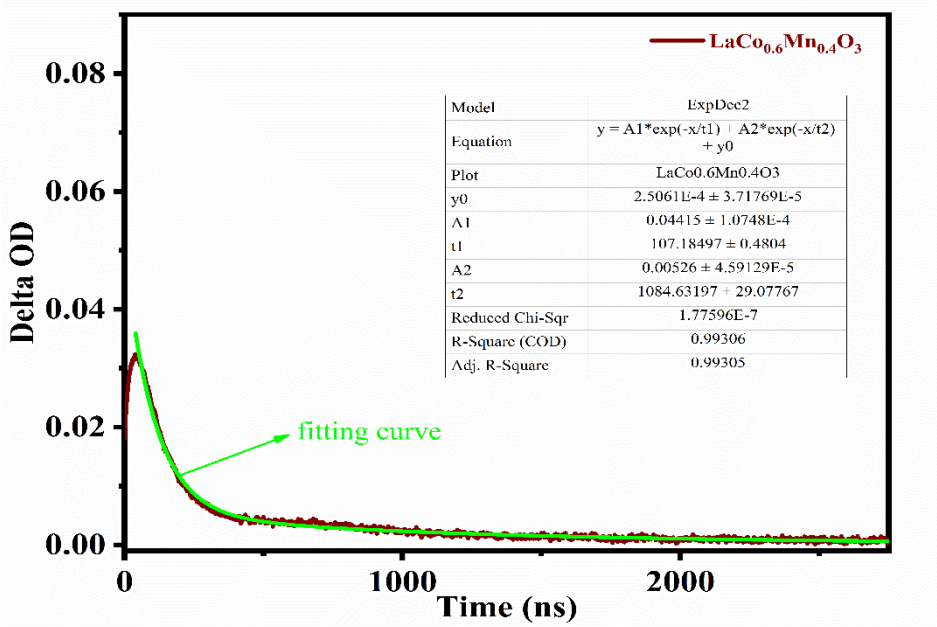

Figure S8. Two exponential decay function and fitting curve of $LaCo_{0.6}Mn_{0.4}O_3$

Model	ExpDec2
Equation	y = A1*exp(-x/t1) + A2*exp(-x/t2) + y0
Plot	LaCoO3
y0	0.00103 ± 2.6581E-5
A1	0.01481 ± 7.61746E-5
t1	69.9736 ± 0.73039
A2	0.0032 ± 5.78295E-5
t2	559.88803 ± 21.53735
Reduced Chi-Sqr	9.0747E-8
R-Square (COD)	0.98476
Adj. R-Square	0.98475

Model	ExpDec2
Equation	y = A1*exp(-x/t1) + A2*exp(-x/t2) + y0
Plot	LaCo0.2Mn0.8O3
y0	1.41012E-4 ± 2.34163E-5
A1	0.04519 ± 6.01022E-5
t1	105.23343 ± 0.28548
A2	0.00356 ± 3.50386E-5
t2	958.25689±30.21458
Reduced Chi-Sqr	9.52156E-8
R-Square (COD)	0.99698
Adj. R-Square	0.99698

Model	ExpDec2
Equation	y = A1*exp(-x/t1) + A2*exp(-x/t2) + y0
Plot	LaCo0.4Mn0.6O3
y0	1.7103E-4 ± 2.07843E-5
A1	0.04565 ± 6.27754E-5
t1	103.60735 ± 0.28612
A2	0.00366 ± 3.65915E-5
t2	1030.28778±42.39984
Reduced Chi-Sqr	8.90735E-8
R-Square (COD)	0.99696
Adj. R-Square	0.99696

Model	ExpDec2
Equation	y = A1*exp(-x/t1) + A2*exp(-x/t2) + y0
Plot	LaCo0.6Mn0.4O3
y0	2.5061E-4 ± 3.71769E-5
A1	0.04415 ± 1.0748E-4
t1	107.18497 ± 0.4804
A2	0.00526 ± 4.59129E-5
t2	1084.63197 ± 29.07767
Reduced Chi-Sqr	1.77596E-7
R-Square (COD)	0.99306
Adj. R-Square	0.99305

Model	ExpDec2
Equation	y = A1*exp(-x/t1) + A2*exp(-x/t2) + y0
Plot	LaCo0.8Mn0.2O3
y0	3.60526E-4 ± 1.91409E-5
A1	0.01539 ± 9.77918E-5
t1	158.98094 ± 1.60866
A2	0.00249 ± 1.00634E-4
t2	810.33213 ± 41.20567
Reduced Chi-Sqr	8.86664E-8
R-Square (COD)	0.98663
Adj. R-Square	0.98663

Model	ExpDec2
Equation	y = A1*exp(-x/t1) + A2*exp(-x/t2) + y0
Plot	LaMnO3
y0	-6.82332E-4 ± 5.28277E-5
A1	0.09307 ± 1.33686E-4
t1	71.84606 ± 0.17762
A2	0.00153 ± 4.06588E-5
t2	929.03713±36.64412
Reduced Chi-Sqr	3.53203E-7
R-Square (COD)	0.99536
Adj. R-Square	0.99536

Model	ExpDec2
Equation	y = A1*exp(-x/t1) + A2*exp(-x/t2) + y0
Plot	LaMn0.2Ni0.8O3
y0	2.44894E-4 ± 5.82163E-5
A1	0.03933 ± 2.04932E-4
t1	106.39159 ± 0.98597
A2	0.00354 ± 9.20399E-5
t2	943.15531 ± 63.78419
Reduced Chi-Sqr	3.92063E-7
R-Square (COD)	0.97623
Adj. R-Square	0.97622

Model	ExpDec2
Equation	y = A1*exp(-x/t1) + A2*exp(-x/t2) + y0
Plot	LaMn0.4Ni0.6O3
y0	-4.97285E-4 ± 8.40508E-5
A1	0.0522 ± 7.58674E-5
t1	103.39602 ± 0.30484
A2	0.00481 ± 4.67219E-5
t2	1005.46824±45.15981
Reduced Chi-Sqr	1.72967E-7
R-Square (COD)	0.99633
Adj. R-Square	0.99632

Model	ExpDec2
Equation	y = A1*exp(-x/t1) + A2*exp(-x/t2) + y0
Plot	LaMn0.6Ni0.4O3
y0	8.0139E-5 ± 2.33041E-4
A1	0.06029 ± 2.30665E-4
t1	95.198 ± 0.54337
A2	0.00483 ± 1.62835E-4
t2	1884.0223 ± 188.55227
Reduced Chi-Sqr	5.16949E-7
R-Square (COD)	0.98461
Adj. R-Square	0.9846

Model	ExpDec2
Equation	y = A1*exp(-x/t1) + A2*exp(-x/t2) + y0
Plot	LaMn0.8Ni0.2O3
y0	5.64194E-4 ± 1.32261E-4
A1	0.03309 ± 1.83352E-4
t1	121.06647 ± 1.3571
A2	0.00384 ± 7.42365E-5
t2	900.01315±21.23
Reduced Chi-Sqr	3.82593E-7
R-Square (COD)	0.97607
Adj. R-Square	0.97606

Model	ExpDec2
Equation	y = A1*exp(-x/t1) + A2*exp(-x/t2) + y0
Plot	LaNiO3
y0	9.35248E-4±1.12567E-5
A1	0.013678±6.45981E-5
t1	83.36753±1.36748
A2	0.00456±5.69341E-5
t2	382.56842±6.47942
Reduced Chi-Sqr	8.76392E-8
R-Square (COD)	0.98956
Adj. R-Square	0.98954

Model	ExpDec2
Equation	y = A1*exp(-x/t1) + A2*exp(-x/t2) + y0
Plot	LaNi0.2Co0.8O3
y0	6.93307E-4 ± 1.10232E-5
A1	0.02666 ± 8.21478E-5
t1	88.76911 ± 0.54262
A2	0.00887 ± 7.70153E-5
t2	573.33585 ± 5.75224
Reduced Chi-Sqr	1.24554E-7
R-Square (COD)	0.99422
Adj. R-Square	0.99421

Model	ExpDec2
Equation	y = A1*exp(-x/t1) + A2*exp(-x/t2) + y0
Plot	LaNi0.4Co0.6O3
y0	2.9362E-4 ± 1.07145E-5
A1	0.02588 ± 1.03069E-4
t1	100.60057 ± 0.55947
A2	0.00498 ± 1.00199E-4
t2	532.30612 ± 10.77637
Reduced Chi-Sqr	1.37458E-7
R-Square (COD)	0.99403
Adj. R-Square	0.99403

Model	ExpDec2
Equation	y = A1*exp(-x/t1) + A2*exp(-x/t2) + y0
Plot	LaNi0.6Co0.4O3
y0	0.00106 ± 2.22346E-5
A1	0.03326 ± 8.64923E-5
t1	95.79422 ± 0.50681
A2	0.00858 ± 5.96548E-5
t2	980.45426±10.78608
Reduced Chi-Sqr	1.7702E-7
R-Square (COD)	0.99353
Adj. R-Square	0.99352

Model	ExpDec2
Equation	y = A1*exp(-x/t1) + A2*exp(-x/t2) + y0
Plot	Ni0.8Co0.2
y0	8.34462E-4 ± 1.63975E-5
A1	0.03634 ± 8.87869E-5
t1	91.82478 ± 0.45433
A2	0.00721 ± 7.42381E-5
t2	955.84573±9.95398
Reduced Chi-Sqr	1.77399E-7
R-Square (COD)	0.99383
Adj. R-Square	0.99382

Figure S9. The error of lifetime of LCMO, LMNO and LNCO